

VIP Very Important Paper

www.batteries-supercaps.org

Enhanced Polysulfides Adsorption and Conversion for High Coulombic Efficiency Sodium-Ion Batteries

Yu-Hua Bian⁺^[a], Xuan-Wen Gao⁺^[a], Lu-Kang Zhao,^[a] Zhaomeng Liu,^[a] Qinfen Gu,^[a, b] and Wen-Bin Luo^{*[a]}

Transition metal sulphides based on conversion reaction mechanism have attracted much attention as anode materials for sodium-ion batteries owing to their theoretical specific capacity and potential long lifespan. The unsatisfactory Coulombic efficiency, however, inhabits the cycling lifespan due to the intermediate polysulfide formation (Na_2S_x ; $4 \leq x \leq 6$) and chain reactions. To enhance the polysulfide polysulfide adsorption capability and capacity, a hybrid with synergistic sodium storage and polysulfide adsorption capability was designed, in which massive CoS_2 nanoparticles (CoS_2 NP) were utilized as electrons supplier to enhance the adsorption energy of three-dimensional nitrogen-doped carbon (3D-NC) framework to-

wards sodium polysulfide. Combining the experimental and computational results, the encapsulated CoS_2 can dramatically optimize the local electronic structure and function as a powerful electron reservoir to increase the effective adsorption to Na_2S_x ($4 \leq x \leq 6$). Meanwhile, the electron transferring between CoS_2 NP and 3D-NC can facilitate the conversion of Na_2S to Na_2S_x . An ultra-high initial Coulombic efficiency of 98.05% and 98.38% can be achieved at current densities of 0.06 A g^{-1} and 0.4 A g^{-1} , respectively. Beneficial from the high reversible capability, a superior cycling lifespan is obtained up to 800 long cycles at current densities of 0.6 A g^{-1} .

Introduction

To overcome the shortage of fossil fuels and the negative impact on the environment, exploring and developing novel rechargeable secondary ion batteries has been considered as one of the most promising solutions, which can accelerate and ameliorate the large-scale energy storage ecosystem.^[1,2] Transition metal sulphides (TMS) have been paid continuous and extensive attention in the field of secondary ion batteries (such as sodium ion battery) owing to the inherent advantages of high-economic efficiency and easily controllable structure.^[3,4] Although possessing a high theoretical specific capacity and potential long lifespan, the critical issues of unsatisfactory Coulombic efficiency and massive non-estimated sides reaction hinder the development of the transition metal sulphide application. The primary reason primarily originates from the intermediate products formation (such as polysulfide) during long-term cycling periods.^[4c,5,6]

Based on the conversion reaction mechanism of transition metal polysulfide in secondary ion batteries, it has been found

that besides the traditional conversion reaction between solid CoS_2 and Na_2S (take CoS_2 in sodium ion battery for example), the solid-liquid phase conversion process occurs simultaneously between the active material and soluble polysulfide sodium (Na_2S_n , $2 < n < 8$) as shown in Figure 1(a, b). Those dissolved intermediate products (sodium polysulfide) can not only lead to a continuous change in electrolyte viscosity and electron/ion conductivity, but also result in a severe loss of active material and a continuous Coulombic efficiency reduction for accelerating the sodium dendrites growth.^[7,8] As can be seen in Figure 1(c) of a cell assembled with sodium metal electrodes and polysulfide (CoS_2 , MoS_2 , FeS_2), there is an obvious absorption signal around 300–400 nm in the electrolyte corresponding to the $\text{Na}_2\text{S}_6/\text{Na}_2\text{S}_4$ formation after several cycles (Figure 1d). Therefore, suppressing the polysulfides formation plays an important and necessary role in improving the sodium storage performance of metal polysulfides in sodium ion batteries (SIBs). It is well-known that polar adsorption sites can adsorb polysulfides and thus suppress the shuttle effect. Nitrogen-doped carbon (NC) was thus commonly used as the sulfur carrier in early metal/sulfur cells to inhibit polysulfide shuttling by physical domain limitation, in addition to further limiting polysulfide solubilization by polar adsorption. However, due to the limited adsorption capacity and capability along with substantial negative sides reactions, subsequent studies had been made by designing massive polar adsorption sites on NC carriers with large surface area, such as oxides.^[6c–e,9] Balance the surface area with Coulombic efficiency and ion storage capability, therefore, become the bottleneck presently which still obstacle the further application.

To enhance the polysulfide adsorption capability and ion storage capacity simultaneously, herein, massive CoS_2 nanoparticles (CoS_2 NP) were utilized as electrons supplier to

[a] Y.-H. Bian,⁺ Prof. X.-W. Gao,⁺ L.-K. Zhao, Dr. Z. Liu, Prof. Q. Gu, Prof. W.-B. Luo

Institute for Energy Electrochemistry and Urban Mines Metallurgy, School of Metallurgy

Northeastern University

Shenyang 110819, China

E-mail: luowenbin@smm.neu.edu.cn

[b] Prof. Q. Gu

Australian Synchrotron (ANSTO)

800 Blackburn Rd, Clayton, Victoria 3168, Australia

[+] These authors contributed equally to this work.

Supporting information for this article is available on the WWW under <https://doi.org/10.1002/batt.202300227>

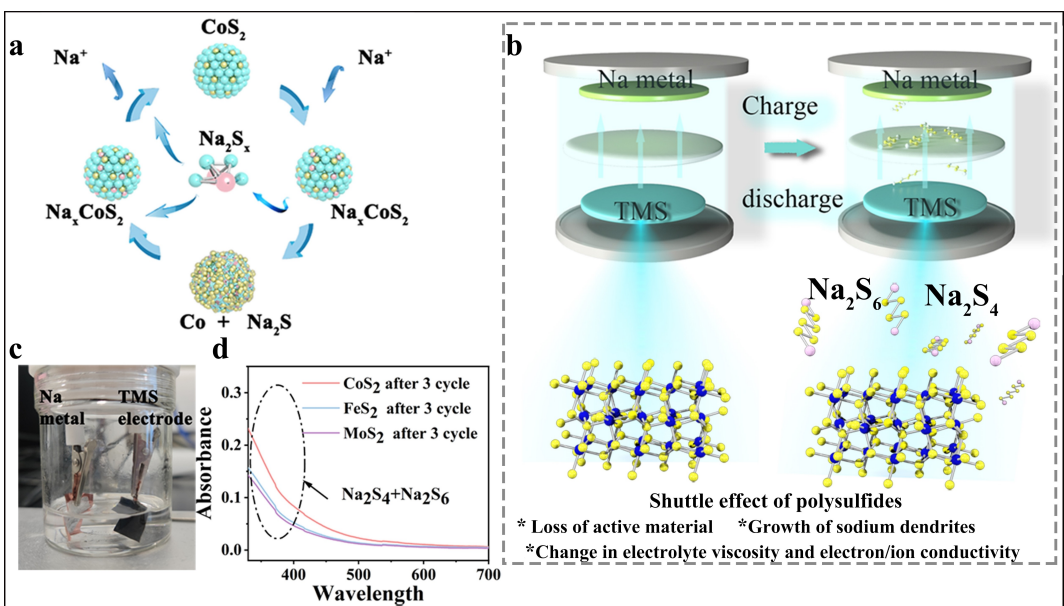


Figure 1. a) Schematic diagram of the reaction pathway for sodium storage in CoS_2 ; b) Schematic representation of the shuttle effect of TMS during charging and discharging; c) Photograph of a cell setup for characterizing polysulfides dissolved in the electrolyte during charging and discharging of TMS electrodes; d) UV-vis spectra of the electrolytes of CoS_2 , MoS_2 and FeS_2 electrodes after one cycle of charge and discharge in the cell respectively.

enhance the adsorption energy of three-dimensional nitrogen-doped carbon (3D-NC) framework towards sodium polysulfide. Density functional theory calculation reveals that the obtained sample can enhance the adsorption energy of polysulfide through electron transferring between CoS_2 NP and 3D-NC, thus inhibiting the shuttle effect. Meanwhile, the electron transfer between CoS_2 NP and 3D-NC can facilitate the conversion of Na_2S to Na_2S_x . Electrochemical tests towards sodium ion batteries (SIBs) illustrate that the hybrid can realize enhanced adsorption on first charge and discharge with an initial Coulombic efficiency of 98.05% at current densities of 0.06 A g^{-1} . At current densities of 0.6 A g^{-1} , there is a stable cycling lifespan for 800 long cycles. This work reveals the close influence of polysulfides on the initial Coulomb efficiency and cycling stability during ions storage in TMS anodes and provides a feasible strategy to improve the reversibility of the long-cycle reactions.

Results and Discussion

As shown the synthesis schematic diagram in Figure S2, the obtained sample was prepared by anchoring massive CoS_2 NP into 3D-NC framework and the detailed information can be seen in the experimental section. Briefly, metal-organic skeleton, cobalt 2-methylimidazole (ZIF-67), was employed as the carbon precursor and synthesized using cobalt nitrate hexahydrate and zinc nitrate hexahydrate. The appropriate amount of zinc elements increases the spatial distance of Co and prevented Co from gathering into large particles at high temperatures. The organic components were converted to nitrogen-doped carbon during carbonization at 900°C . The final sample (simply named as CoS_2 NP@3D-NC) were obtained by

sulfurizing at 400°C . The evaporated zinc could produce abundant micropores, which increase the sodium ion diffusion path and provide richer adsorption sites for polysulfide.^[10] The XRD patterns of pure CoS_2 and CoS_2 NP@3D-NC are exhibited in Figure S3(a). The diffraction peaks at 32.3° , 36.2° , 46.3° , 49.3° , and 54.9° are attributed to the (200), (210), (211), (220), and (311) planes of CoS_2 , respectively (JCPDS no. 41–1471),^[11] indicating that the particles were fully sulfurized. The morphology and microstructure of CoS_2 NP@3D-NC were observed by Field Emission Scanning Electron Microscope (FESEM) and high-resolution transmission electron microscope (HRTEM) as shown in Figure S4(a, b). It can be clearly seen that the morphology of CoS_2 NP@3D-NC is a regular and similar orthorhombic dodecahedron with ZIF-67. Massive CoS_2 nanoparticles are distributed inside the carbon dodecahedron, the excellent spatial layout provides a fast channel for ion diffusion with exposing a large amount of adsorption sites.^[10b] EDX analysis (Figure S4c) confirmed the presence and uniform distribution of Co, S, C and N elements on the surface of CoS_2 NP@3D-N.^[9c]

Density function theory (DFT) calculation was carried out priority to evaluate the polysulfides adsorption energy on both nitrogen-doped carbon (Figure S5) and CoS_2 NP@3D-NC (Figure 2). A layer of nitrogen doped carbon and the $\text{CoS}_2(100)$ model are presented as models, while as a comparison, a layer of nitrogen doped carbon model is simultaneously calculated as a reference. Adsorption energy calculation results show that the adsorption energies (E_{ad}) of 0.792 eV , 0.722 eV and 0.720 eV for Na_2S , Na_2S_4 and Na_2S_6 adsorption on CoS_2 NP@3D-NC, respectively, are both higher than those of 0.599 eV , 0.721 eV and 0.692 eV for Na_2S , Na_2S_4 and Na_2S_6 adsorption on NC, respectively. By comparing the electron depletion and aggregation around Na_2S_x , it is concluded that the CoS_2 existence can dramatically enhance the interaction of Na_2S_x with NC. Mean-

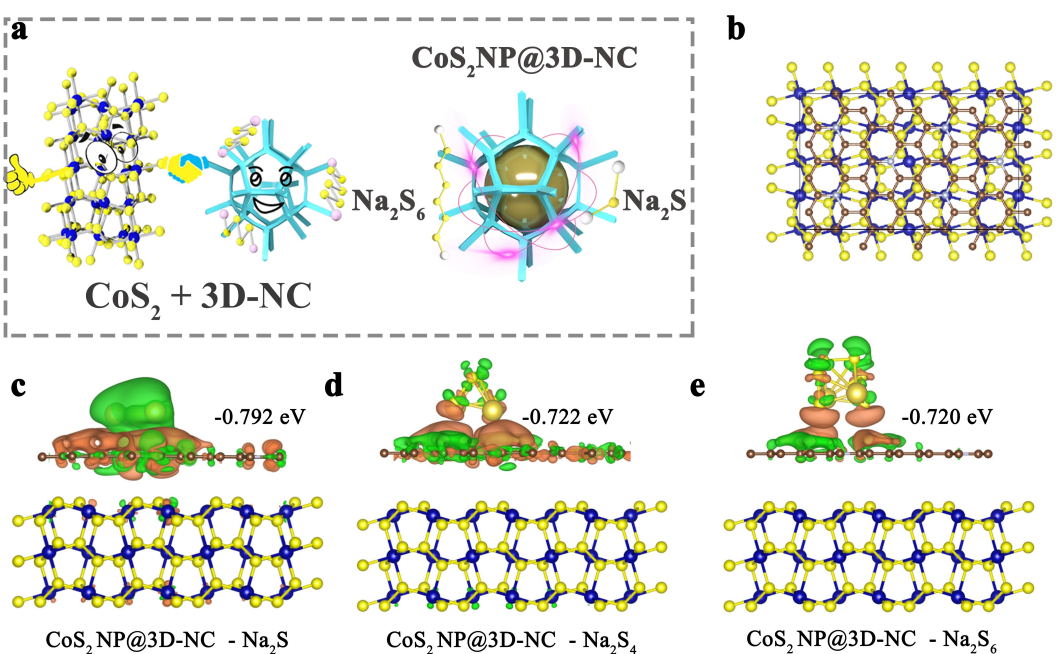


Figure 2. a) Schematic representation of the synergistic adsorption of CoS_2 NP and 3D-NC. b) DFT calculation model for CoS_2 NP@3D-NC. Adsorptive energies and differential charge density (DCD) diagrams of CoS_2 NP@3D-NC to; c) Na_2S ; d) Na_2S_4 ; e) Na_2S_6 .

while, Na_2S_x can be effectively adsorbed onto CoS_2 NP@3D-NC and synergistically promote the multi-step conversion of Na_2S_x .^[6d,e]

In order to analyze the surface electronic state and chemical composition of CoS_2 NP@3D-NC, X-ray photoelectron spectroscopy (XPS) test was performed as shown in Figure 3 and Figure S6. The complete XPS spectrum shows that Co, S, C, and N are predominantly present in the material.^[12] Figure 3(a) shows the C 1s spectrum, in which four peaks are available at 284.4 eV (C–C bond), 285.3 eV (C=C bond), 287.3 eV (C–N bond) and 290.8 eV (C–O–C bond).^[9c] N 1s spectra (Figure 3b) are available with anti-fold products of 398.9 eV, 400.5 eV and 401.4 eV for other peaks that are attributed to pyridine N, pyrrolic N and graphite N respectively.^[2a] In the Co 2p spectra (Figure 3c), the Co 2p core layer contains a Co 2p_{3/2} and a Co 2p_{1/2} component, each of which can be further anti-folded into two pairs of spin-orbit binaries and two vibrational satellites. CoS_2 NP@3D-NC are the doublets at 778.9/794.5, 780.4/796.7 and 782.6/802.6 eV are assigned to Co^{3+} , Co^{2+} , and the satellite peaks, respectively.^[13] The S 2p spectrum (Figure 3d) can be fitted to the three peaks at 163.8 eV (S 2p_{3/2}), 165.0 eV (S 2p_{1/2}) and 168.3 eV.^[13]

The characteristic peaks of carbon in CoS_2 NP@3D-NC were evaluated by Raman spectroscopy as shown in Figure S3(b). The characteristic peaks at around 1591.1 and 1348.4 cm⁻¹ correspond to the G and D bands.^[14] The content of each component in CoS_2 NP@3D-NC was tested by thermogravimetric analysis (TGA) (Figure S3c). As can be calculated, the mass loss of the first part is mainly from the oxidation of carbon while the mass loss of the second part is from the complete oxidation of cobalt disulfide. After calculating the mass content of CoS_2 in CoS_2 NP@3D-NC, the weight ratio is about 54.4 wt%. According to

the nitrogen adsorption-desorption isotherms, the specific surface area of the prepared materials was further analyzed and the results are shown in Figure S7. The results indicate that the CoS_2 NP@3D-NC sample has a reasonable specific surface area ($116.4 \text{ m}^2 \text{ g}^{-1}$) and pore volume ($0.336 \text{ cm}^3 \text{ g}^{-1}$). The substantial exposed adsorption sites satisfy the fast immobilization for shuttled polysulfide, while the micropores provide a fast transport network for electrolyte permeation.^[15]

The polysulfide adsorption phenomenon and mechanism were monitored and explored over a potential range of 0.01–3 V (vs. Na^+/Na) as shown in Figure 4. To test the adsorption capacity of CoS_2 NP@3D-NC towards polysulfide, the absorption peak intensities of CoS_2 NP@3D-NC and CoS_2/NC (A physical hybrid of CoS_2 and NC with relatively small negligible CoS_2 and NC interactions) towards Na_2S_6 were determined by UV-Vis spectroscopy. A yellow solution was prepared as shown in Figure 4(a) by dissolve Na_2S_6 into dimethoxyethane (DME). CoS_2 NP@3D-NC and CoS_2/NC were added into to monitor the adsorption phenomenon. The Na_2S_6 solution with the addition of CoS_2 NP@3D-NC powder changed from dull yellow to colorless, while the Na_2S_6 solution with the addition of CoS_2/NC became slightly lighter in color, indicating a much more efficient adsorption of Na_2S_6 on CoS_2 NP@3D-NC.

Figure 4(b) shows the initial three cyclic voltammetry curves using cyclic voltammetry (CV) at a scan rate of 0.1 mV s^{-1} over a potential range of 0.01–3 V. A large peak can be observed at 1.17 V and 1.0 V for CoS_2 NP@3D-NC and CoS_2/NC , respectively, which is attributed to the insertion of sodium ions between the CoS_2 layers and the formation of a solid electrolyte interface (SEI) film. The corresponding reduction peaks at 0.76–0.40 V represent CoS_2 conversion reactions.^[7a] The corresponding reactions are

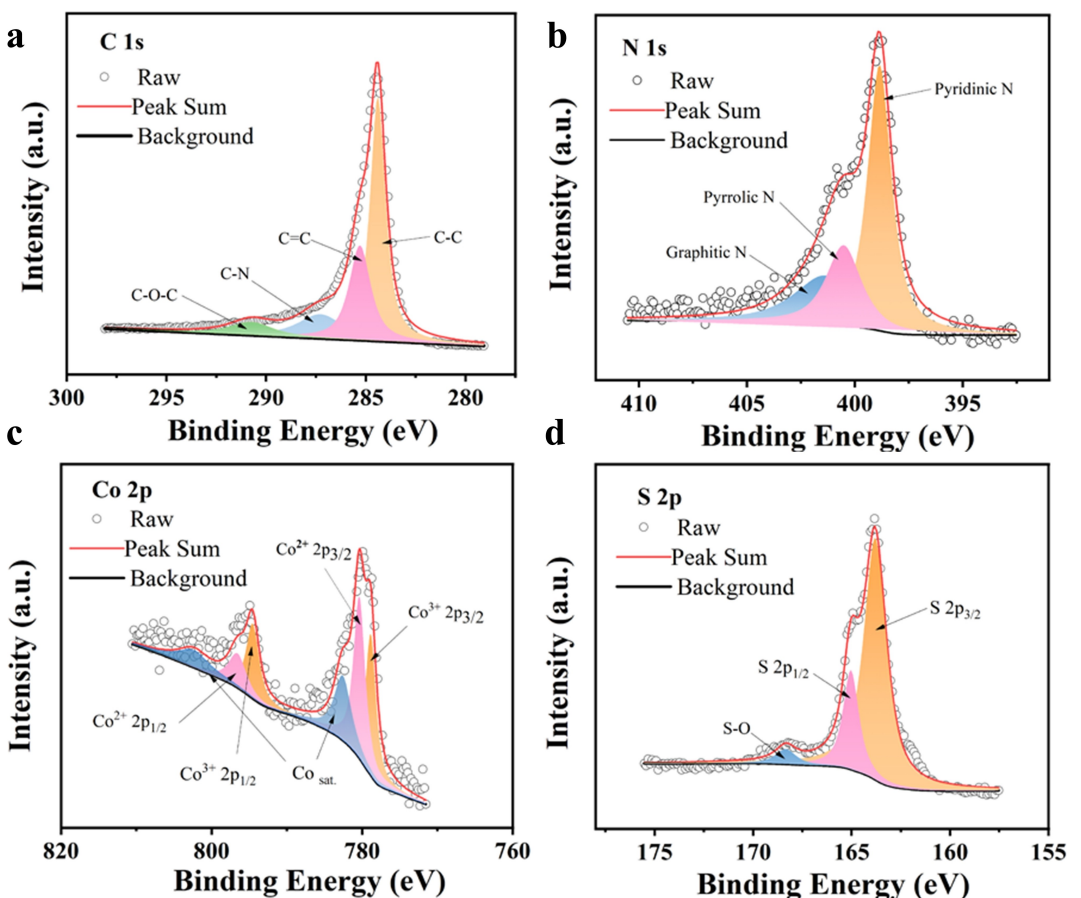
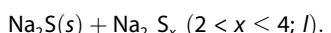
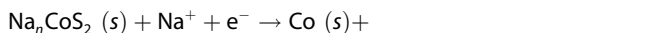
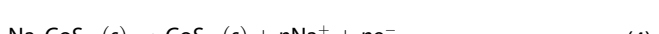
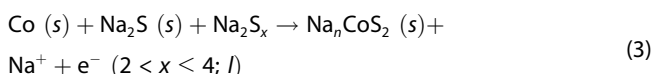


Figure 3. a) C 1s XPS spectrum. b) N 1s XPS spectrum. c) Co 2p XPS spectrum. d) S 2p spectrum of CoS₂ NP@3D-NC.



During the charging of CoS₂ NP@3D-NC, the oxidation peaks at 1.76–2.12 V represent the reversible conversion and sodium ion decalation, and the corresponding reactions are



The ratio of the integral areas of the reduction and oxidation peaks can correspond to the ratio of the specific capacity released by the reduction and oxidation reactions. It is concluded that about 97.77% and 85.53% for CoS₂ NP@3D-NC and CoS₂/NC, respectively. It demonstrates the higher reversibility of the first charge/discharge reaction of CoS₂ NP@3D-NC. After the initial cycle, CoS₂ NP@3D-NC and CoS₂/NC showed new oxidation peaks at 1.5–1.46 V and 1.40 V, respectively, which belong to the conversion reaction of the long-chain polysulfide Na₂S_y (4 < y < 8, l).^[16] Compared with CoS₂/NC, the

oxidation peaks of CoS₂ NP@3D-NC are all closer to the right and the reduction peaks are all closer to the left, especially the reduction peak involving polysulfide conversion at 1.53 V is 0.23 V earlier than that of CoS₂/NC at 1.76 V, indicating that CoS₂ NP@3D-NC is more favorable for the adsorption-transformation of polysulfides.^[10b]

To investigate the dissolution of polysulfide in the electrolyte after the first charge/discharge, the cells were disassembled and the CoS₂ NP@3D-NC and CoS₂/NC anodes were immersed in DME solution for 2 hours respectively. The UV-Vis spectra of both solutions were tested as shown in Figure 4(c). The UV-Vis spectra of the CoS₂/NC soaked solution showed a distinct Na₂S₆/Na₂S₄ peak near 300–500 nm. The UV-Vis spectrum of the CoS₂ NP@3D-NC infiltrated solution shows a weaker peak intensity, which proves that the CoS₂ NP@3D-NC electrode has a better adsorption effect on sodium polysulfide during the first charge and discharge, preventing the loss of active material and thus possessing a higher reversibility of the reaction.^[6a,16]

The conversion of insoluble short-chain NaPSs (such as Na₂S₂ and Na₂S) is another additional intermediate for the slow electrochemical reactions.^[6c,e] In above reaction, this difficult conversion of Na₂S exists, corresponding to the first peak potential during charging, while the reaction potential of CoS₂ NP@3D-NC is 0.23 V ahead of that of CoS₂/NC. To explore this phenomenon, the Bader charges for Na₂S₆, Na₂S₄ and Na₂S

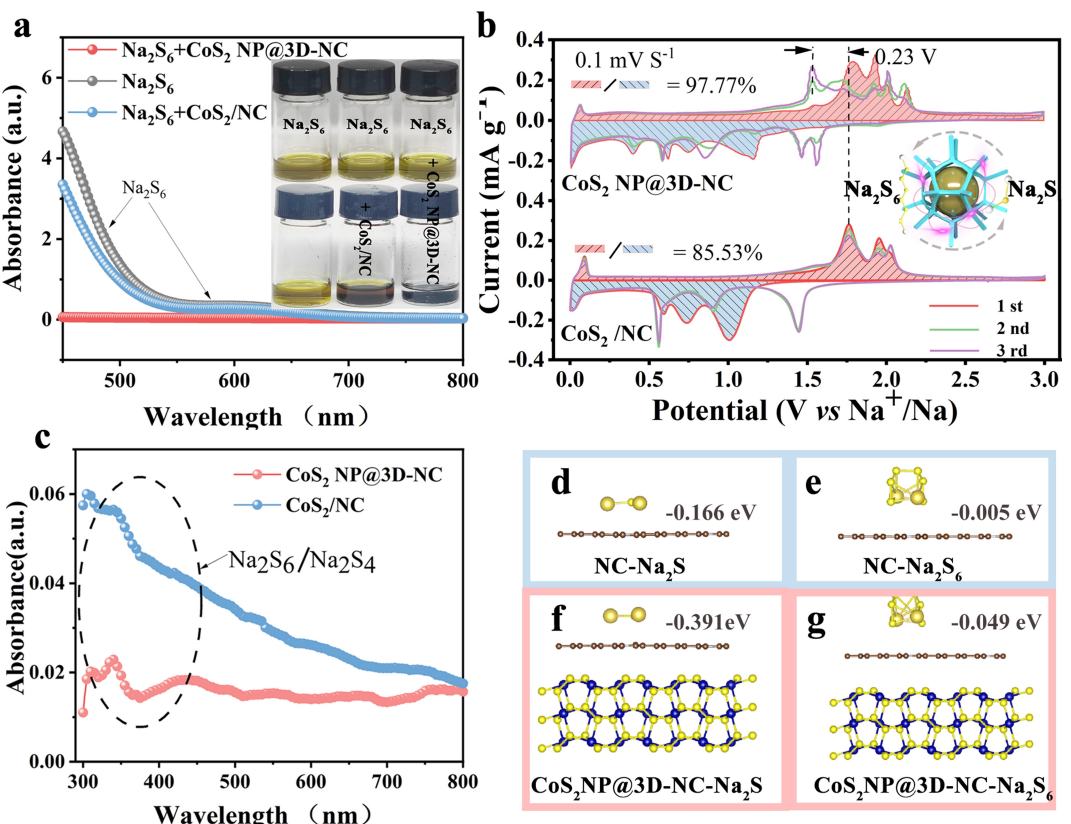


Figure 4. a) UV-Vis adsorption spectra of Na_2S_6 solutions after addition of $\text{CoS}_2 \text{ NP@3D-NC}$ and CoS_2/NC and optical photographs; b) Cyclic voltammograms of the $\text{CoS}_2 \text{ NP@3D-NC}$ and CoS_2/NC with a scan rate of 0.1 mV s^{-1} , the inset shows the adsorption and transformation of NaPSs on $\text{CoS}_2 \text{ NP@3D-NC}$; c) UV-Vis adsorption spectra of the electrolyte at 300 nm after the first cycle. Bader charges for d) Na_2S and e) Na_2S_6 adsorption on NC. Bader charges for f) Na_2S and g) Na_2S_6 adsorption on $\text{CoS}_2 \text{ NP@3D-NC}$.

adsorbed on $\text{CoS}_2 \text{ NP@3D-NC}$ and CoS_2/NC were calculated further, respectively. The results showed that the Bader charges of Na_2S adsorbed on NC (Figure 4d) and $\text{CoS}_2 \text{ NP@3D-NC}$ (Figure 4f) were -0.166 eV and -0.391 eV , respectively. The Bader charges of Na_2S_4 adsorbed on NC (Figure S8a) and $\text{CoS}_2 \text{ NP@3D-NC}$ (Figure S8b) were -0.048 eV and -0.073 eV , respectively, and the Bader charges of Na_2S_6 adsorbed on NC (Figure 4e) and $\text{CoS}_2 \text{ NP@3D-NC}$ (Figure 4g) with charges of -0.005 eV and -0.049 eV , respectively. This result suggests that $\text{CoS}_2 \text{ NP@3D-NC}$ is more likely to gain electrons from Na_2S , Na_2S_4 and Na_2S_6 , thus facilitating the oxidation reaction during charging and allowing the reversible conversion of the polysulfide produced by the discharge to occur more fully. In particular, the solid intermediate product Na_2S is more likely to lose electrons during charging to soluble polysulfides that are susceptible to conversion reactions.^[17] The accelerated reaction kinetics allows the reaction potential to be advanced by 0.23 V . It further confirms that the synergistic action of CoS_2 particles with 3D-NC during charging and discharging has favored the repositioning of electrons, optimizing the charge density and catalyzing the redox reaction of polysulfides (shown in the inset of Figure 4b).

The enhanced initial Coulomb efficiency (ICE) can be clearly detected as shown in Figure 5(a, b) as well. The discharge specific capacity of $\text{CoS}_2 \text{ NP@3D-NC}$ can reach 580.9 mAh g^{-1}

when discharged to 0.01 V and 569.6 mAh g^{-1} when charged to 3 V at current density of 60 mA g^{-1} , with an ICE of 98.05% , showing a very high reversibility of the reaction. When the current density increased to 0.4 A g^{-1} , the ICE of $\text{CoS}_2 \text{ NP@3D-NC}$ can still keep 98.38% . Beneficial from the high Coulomb efficiency, $\text{CoS}_2 \text{ NP@3D-NC}$ exhibit a superior rate capability as shown in Figure 5(c). The average reversible specific capacities of 569.6 , 562.0 , 548.2 , 536.7 , 517.3 and 487.8 mAh g^{-1} can be released at the current densities of 60 , 120 , 300 , 600 , 1200 and 3000 mA g^{-1} , respectively. The high reversible capacity of 577.5 mAh g^{-1} can be still reached when the current density returned to 60 mA g^{-1} , exceeding the first reversible capacity of 569.6 mAh g^{-1} .

The charging and discharging curves of $\text{CoS}_2 \text{ NP@3D-NC}$ shows an extremely small polarization voltage and specific capacity decay even at a current density of 3 A g^{-1} (Figure 5d). This is also demonstrated by the cycling stability tests of $\text{CoS}_2 \text{ NP@3D-NC}$ at current densities of 0.6 A g^{-1} and 1.2 A g^{-1} in Figure 5(e). The $\text{CoS}_2 \text{ NP@3D-NC}$ can keep high 653.8 mAh g^{-1} specific capacity after 800 long cycles at a current density of 0.6 A g^{-1} . The increase in specific capacity during cycling is attributed to the release of active sites after CoS_2 activation. When the current density increased to 1.2 A g^{-1} , the reversible capacity was still keeping 472.3 mAh g^{-1} after 800 long cycles. Figure 5(f) compares the ICE of some transition metal sulphides

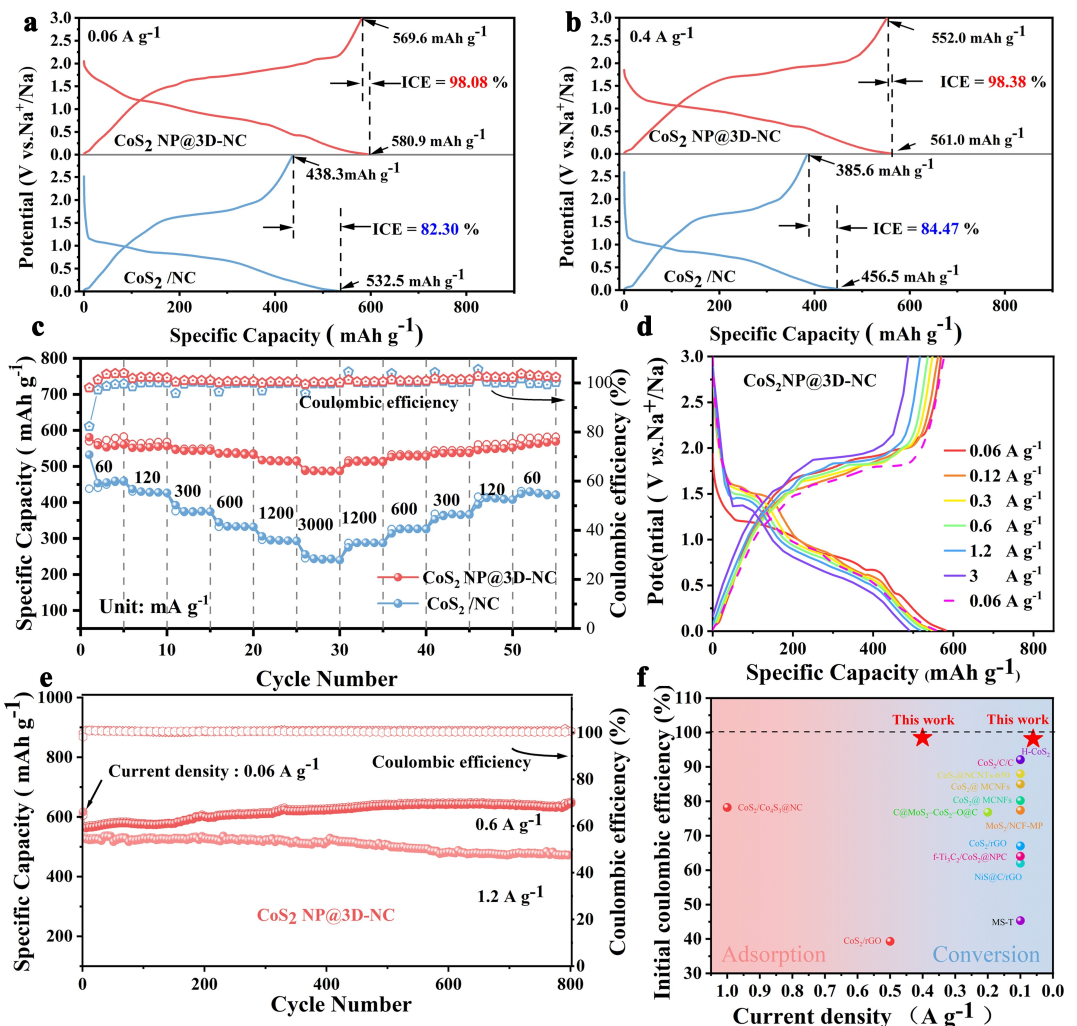


Figure 5. The first charge/discharge curve of CoS₂ NP@3D-NC and CoS₂ /NC at current density of a) 0.06 A g⁻¹ and b) 0.4 A g⁻¹. c) Rate performance and d) discharge/charge curves for different current densities of CoS₂ NP@3D-NC; e) cycling performance of CoS₂ NP@3D-NC at 0.6 A g⁻¹, 1.2 A g⁻¹; f) the initial coulombic efficiency comparison chart.^[4d,9d,f,13,18]

when used as anode materials for sodium ion batteries, the highest ICE can be achieved among known metal sulphide anodes. Based on the above results, it is concluded that CoS₂ nanoparticles in CoS₂ NP@3D-NC can act as a powerful electron reservoir to provide electron exchange for the adsorption sites of polysulfides under the solid-liquid phase conversion mechanism of polysulfides. Meanwhile, the CoS₂ NP@3D-NC traps the dissolution of polysulfide in the electrolyte, preventing the loss of active material while facilitating the conversion of polysulfide.

To investigate the Na⁺ reaction kinetics and storage mechanisms, CV measurements were performed at different scan rates (0.1–5.0 mV s⁻¹) as shown in Figure 6(a). The position of the main peak of the CoS₂ NP@3D-NC electrode showed a smaller change with increasing scan rate, indicating that the electrode only underwent a very small polarization. Figure S11 shows that the fitted *b* values of peak 1 to peak 6 of the CoS₂ NP@3D-NC and CoS₂ /NC electrode, indicating more contribution from surface reactions during cycling.^[9b,e,14,18] As shown in Figure 6(b, c), the pseudo-capacitance contribution of CoS₂

NP@3D-NC was significantly higher than that of CoS₂ /NC at different scan rates, which was attributed to the special structure of CoS₂ NP@3D-NC that enhanced the adsorption conversion of polysulfides and improved the sodium ion reaction kinetics.

To further investigate the resistance and sodium diffusion coefficient, the *in-situ* electrochemical impedance spectroscopy (EIS) was carried out as shown in Figure 6(d–g). The total resistance (R_{tot}) is calculated as the sum of the interface resistance^[19] and the charge transfer resistance, and the pattern of R_{tot} with potential is analyzed in Figure 6(f) and Table S1. In Table S2, the slope of CoS₂ NP@3D-NC at each potential is calculated by plotting the line between Z'' and $W_{1/2}$ to obtain σ , which is used to calculate the diffusion coefficient. In Figure 6(g), the trend of sodium diffusion coefficients for CoS₂ NP@3D-NC and CoS₂ /NC is generally the same as the voltage changes. However, CoS₂ NP@3D-NC has a higher sodium ion diffusion coefficient due to its fine structural design and less sodium polysulfide diffusion.

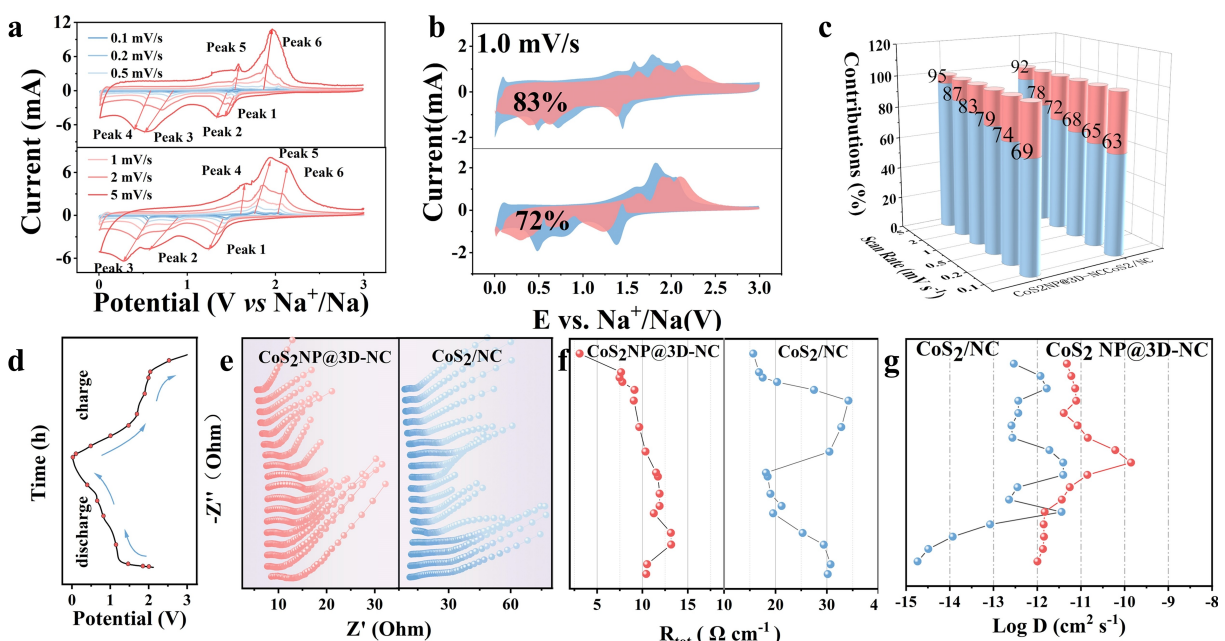


Figure 6. CoS_2 NP@3D-NC and CoS_2 /NC: a) CV curves at different scan rates; b) the CV curve with capacitance contribution shown in the shaded area at 1.0 mV s^{-1} ; c) capacitance contribution ratio at different scans rates ; d) *In-situ* EIS test potential in first charge/discharge ; e) Nyquist plots of the impedance spectra within frequency range from 100 kHz to 0.1 Hz ; f) R_{tot} trend graph; g) Na ion diffusion coefficient trend graph.

Conclusions

By analyzing the causes of transition metal sulphide irreversible ion storage with a low Coulombic efficiency, it is found that besides the traditional conversion reaction, the solid-liquid phase conversion process occurs simultaneously between the active material and soluble polysulfide sodium (Na_2S_n , $2 < n < 8$). In order to enhance the polysulfide adsorption capability and capacity, herein, a hybrid with synergistic sodium ions storage and polysulfide adsorption capability was designed and synthesized successfully, in which massive CoS_2 nanoparticles (CoS_2 NP) were utilized as electrons supplier to enhance the adsorption energy of three-dimensional nitrogen-doped carbon (3D-NC) framework towards sodium polysulfide. The introduced CoS_2 NP can dramatically optimize the local electronic structure and function as a powerful electron reservoir to increase the effective adsorption to Na_2S_x ($4 \leq x \leq 6$). Meanwhile, the electron transferring between CoS_2 NP and 3D-NC can facilitate the conversion of Na_2S to Na_2S_x . The initial Coulomb efficiency of sodium ion reversible storage can reach up to 98. 05% and 98.38% at current densities of 0.06 A g^{-1} and 0.4 A g^{-1} . Beneficial from the high reversible capability, a superior cycling lifespan is obtained up to 800 long cycles at current densities of 0.6 A g^{-1} . By exploring the issues of irreversible ion storage, this work could provide an effective pathway to control the shuttle behavior of the intermediate products for transition metal polysulfide.

Supporting Information

Supporting Information is available from the Wiley Online Library or from the author.

Acknowledgements

This work was supported by the National Natural Science Foundation of China (Grant No. 52272194), LiaoNing Revitalization Talents Program (Grant No. XLYC2007155). Great thanks to A/Prof. Guoping Gao's great contribution to the calculation. This manuscript was written through the contributions of all the authors. All authors have given approval to the final version of the manuscript.

Conflict of Interests

The authors declare no conflict of interest.

Data Availability Statement

The data that support the findings of this study are available from the corresponding author upon reasonable request.

Keywords: sodium-ion battery • anode • transition metal sulphide • polysulfide • Coulombic efficiency

- [1] a) P. K. Nayak, L. Yang, W. Brehm, P. Adelhelm, *Angew. Chem. Int. Ed.* **2018**, *57*, 102–120; b) T. M. Gür, *Energy Environ. Sci.* **2018**, *11*, 2696–2767.
- [2] a) L. Cao, X. Gao, B. Zhang, X. Ou, J. Zhang, W.-B. Luo, *ACS Nano* **2020**, *14*, 3610–3620; b) Q. Zhang, X.-W. Gao, Y. Shi, W.-B. Luo, Y. Li, Q.-F. Gu, H.-N. Fan, F. Li, H.-K. Liu, *Energy Storage Mater.* **2021**, *39*, 54–59.
- [3] a) S. H. Qi, D. X. Wu, Y. Dong, J. Q. Liao, C. W. Foster, C. O'Dwyer, Y. Z. Feng, C. T. Liu, J. M. Ma, *Chem. Eng. J.* **2019**, *370*, 185–207; b) J. He, A. Bhargav, W. Shin, A. Manthiram, *J. Am. Chem. Soc.* **2021**, *143*, 20241–20248.
- [4] a) Y. J. Fang, B. Y. Guan, D. Y. Luan, X. W. Lou, *Angew. Chem. Int. Ed.* **2019**, *58*, 7739–7743; b) Z. X. Lu, Y. J. Zhai, N. N. Wang, Y. H. Zhang, P. Xue, M. Q. Guo, B. Tang, D. Huang, W. X. Wang, Z. C. Bai, S. X. Dou, *Chem. Eng. J.* **2020**, *380*, 122455; c) H. Xia, L. Zan, P. Yuan, G. Qu, H. Dong, Y. Wei, Y. Yu, Z. Wei, W. Yan, J.-S. Hu, D. Deng, J.-N. Zhang, *Angew. Chem. Int. Ed.* **2023**, *62*, e202218282; d) Z. Y. Song, G. Wang, Y. Chen, Q. Chang, Y. Lu, Z. Y. Wen, *Chem. Eng. J.* **2022**, *435*, 134633; e) K. Pan, Y. Sun, X. He, F. Lai, H. Wang, L. Liang, Q. Li, X. Zhang, H. Ji, *RSC Adv.* **2021**, *11*, 17332–17339; f) J. Liu, T. Zhou, T. Han, L. Zhu, Y. Wang, Y. Hu, Z. Chen, *Chem. Commun.* **2022**, *58*, 5108–5111; g) X. Y. Jiang, T. Cao, F. Zhang, J. H. Zhang, K. Qin, H. M. Liu, Y. Y. Xia, *ACS Appl. Energ. Mater.* **2021**, *4*, 6874–6882.
- [5] a) A. A. Razzaq, X. Yuan, Y. Chen, J. Hu, Q. Mu, Y. Ma, X. Zhao, L. Miao, J.-H. Ahn, Y. Peng, Z. Deng, *J. Mater. Chem. A* **2020**, *8*, 1298–1306; b) Y. P. Liu, S. Y. Ma, L. F. Liu, J. L. Koch, M. Rosebrock, T. R. Li, F. Bettels, T. He, H. Pfnnur, N. C. Bigall, A. Feldhoff, F. Ding, L. Zhang, *Adv. Funct. Mater.* **2020**, *30*, 2002462.
- [6] a) M. Jirong, L. Yijuan, O. Liji, H. Jianlin, *Energy Storage Mater.* **2022**, *52*, 111–119; b) F. Xiao, H. Wang, T. Yao, X. Zhao, X. Yang, D. Y. W. Yu, A. L. Rogach, *ACS Appl. Mater. Interfaces* **2021**, *13* (15), 18010–18020; c) M. Wang, H. Zhang, W. Zhang, Q. Chen, K. Lu, *Small Methods* **2022**, *6*, 2200335; d) Y. X. Wang, W. H. Lai, S. L. Chou, H. K. Liu, S. X. Dou, *Adv. Mater.* **2020**, *32*, 1903952; e) Z. Yang, R. Xiao, X. Zhang, X. Wang, D. Zhang, Z. Sun, F. Li, *Energy Environ. Mater.* **2022**, *5*, 693–710; f) Y. Zhang, P. Wang, Y. Yin, X. Zhang, L. Fan, N. Zhang, K. Sun, *Chem. Eng. J.* **2019**, *356*, 1042–1051.
- [7] a) X. Yin, Y. Ren, S. Guo, B. Sun, L. Wu, C. Du, J. Wang, G. Yin, H. Huo, *Adv. Funct. Mater.* **2022**, *32*, 2110017; b) X. Yin, Y. Ren, L. Wu, Z. Zhang, C. Du, J. Wang, G. Yin, H. Huo, *J. Energy Chem.* **2022**, *71*, 210–217; c) H. Tao, M. Zhou, R. Wang, K. Wang, S. Cheng, K. Jiang, *Adv. Sci. Sci.* **2018**, *5*, 1801021.
- [8] M. Hu, Z. Ju, Z. Bai, K. Yu, Z. Fang, R. Lv, G. Yu, *Small Methods* **2019**, *4*, 1900673.
- [9] a) X. Liu, K. Zhang, K. Lei, F. Li, Z. Tao, J. Chen, *Nano Res.* **2016**, *9*, 198–206; b) Y. Liu, Z. Chen, H. Jia, H. Xu, M. Liu, R. Wu, *ACS Nano* **2019**, *13*, 6113–6124; c) W. F. Miao, Y. Zhang, H. T. Li, Z. H. Zhang, L. Li, Z. Yu, W. M. Zhang, *J. Mater. Chem. A* **2019**, *7*, 5504–5512; d) Y. Pan, X. Cheng, L. Gong, L. Shi, T. Zhou, Y. Deng, H. Zhang, *ACS Appl. Mater. Interfaces* **2018**, *10*, 31441–31451; e) F. Xiao, *ACS Appl. Mater. Interfaces* **2020**, *12* (49), 54644–54652; f) K. Xie, L. Li, X. Deng, W. Zhou, Z. Shao, *J. Alloys Compd.* **2017**, *726*, 394–402; g) M. Wang, L. Fan, D. Tian, X. Wu, Y. Qiu, C. Zhao, B. Guan, Y. Wang, N. Zhang, K. Sun, *ACS Energy Lett.* **2018**, *3* (7), 1627–1633.
- [10] a) J. Zhao, X. Quan, S. Chen, Y. Liu, H. Yu, *ACS Appl. Mater. Interfaces* **2017**, *9* (34), 28685–28694; b) C. Ma, Y. Zhang, Y. Feng, N. Wang, L. Zhou, C. Liang, L. Chen, Y. Lai, X. Ji, C. Yan, W. Wei, *Adv. Mater.* **2021**, *33*, 2100171.
- [11] a) L. Chen, N. J. Luo, S. P. Huang, Y. F. Li, M. D. Wei, *Chem. Commun.* **2020**, *56*, 3951–3954; b) Z. Li, W. Feng, Y. Lin, X. Liu, H. Fei, *RSC Adv.* **2016**, *6*, 70632–70637.
- [12] J. Ruan, Y. Pang, S. Luo, T. Yuan, C. Peng, J. Yang, S. Zheng, *J. Mater. Chem. A* **2018**, *6*, 20804–20812.
- [13] P. Huang, H. Ying, S. Zhang, Z. Zhang, W.-Q. Han, *Chem. Eng. J.* **2022**, *429*, 1385–8947.
- [14] X. Ou, Z. Xiao, J.-f. Zhang, C. Wang, D. Wang, B. Zhang, Y. Wu, *ACS Nano* **2020**, *14* (10), 13952–13963.
- [15] a) Y. Pan, *ACS Appl. Mater. Interfaces* **2017**, *9* (41), 35820–35828; b) J. Ruan, F. Mo, Z. Long, Y. Song, F. Fang, D. Sun, S. Zheng, *ACS Nano* **2020**, *14*, 12222–12233.
- [16] E. Zhang, X. Hu, L. Meng, M. Qiu, J. Chen, Y. Liu, G. Liu, Z. Zhuang, X. Zheng, L. Zheng, Y. Wang, W. Tang, Z. Lu, J. Zhang, Z. Wen, D. Wang, Y. Li, *J. Am. Chem. Soc.* **2022**, *144* (41), 18995–19007.
- [17] Y. Lei, C. Wu, X. Lu, W. Hua, S. Li, Y. Liang, H. Liu, W.-H. Lai, Q. Gu, X. Cai, N. Wang, Y.-X. Wang, S.-L. Chou, H.-K. Liu, G. Wang, S.-X. Dou, *Angew. Chem. Int. Ed.* **2022**, *61*, 202200384.
- [18] a) A. Cheng, H. Y. Zhang, W. H. Zhong, Z. P. Li, D. J. Cheng, Y. X. Lin, Y. D. Tang, H. Y. Shao, Z. H. Li, *Carbon* **2020**, *168*, 691–700; b) C. F. Dong, L. J. Guo, H. B. Li, B. Zhang, X. Gao, F. Tian, Y. T. Qian, D. B. Wang, L. Q. Xu, *Energy Storage Mater.* **2020**, *25*, 679–686; c) Z. Li, W. Feng, Y. Lin, X. Liu, H. Fei, *RSC Adv.* **2016**, *6*, 70632–70637; d) X. Liu, K. Zhang, K. Lei, F. Li, Z. Tao, J. Chen, *Nano Res.* **2016**, *9*, 198–206; e) Y. Pan, X. Cheng, Y. Huang, L. Gong, H. Zhang, *ACS Appl. Mater. Interfaces* **2017**, *9* (41), 35820–35828; f) Y. Y. Wang, S. M. Sun, Y. Jiang, Q. Cai, Y. H. Zhang, L. M. Zhou, S. M. Fang, J. Liu, Y. Yu, *ACS Nano* **2020**, *14*, 15577–15586; g) F. Xiao, X. Yang, D. Wang, H. Wang, D. Y. W. Yu, A. L. Rogach, *ACS Appl. Mater. Interfaces* **2020**, *12*, 12809–12820; h) Z. Zhang, Y. Huang, X. Gao, Z. Xu, X. Wang, *ACS Appl. Energ. Mater.* **2020**, *3* (7), 6205–6214; i) J. Zong, F. Wang, C. Nie, M. Zhao, S. Yang, *J. Mater. Chem. A* **2022**, *10*, 10651–10661.
- [19] a) P. Gi Dae, P. Jin-Sung, K. Jin Koo, K. Yun Chan, *Chem. Eng. J.* **2021**, *428*, 131051; b) R. R. Gaddam, L. Katzenmeier, X. Lamprecht, A. S. Bandarenka, *Phys. Chem. Chem. Phys.* **2021**, *23*, 12926–12944; c) Q. Zhang, J. Luan, Y. Tang, X. Ji, H. Wang, *Angew. Chem. Int. Ed.* **2020**, *59*, 13180–13191.

Manuscript received: July 6, 2023

Revised manuscript received: August 1, 2023

Accepted manuscript online: August 7, 2023

Version of record online: September 1, 2023